Nanoscale Advances

ROYAL SOCIETY OF CHEMISTRY

PAPER

View Article Online
View Journal | View Issue

Cite this: *Nanoscale Adv.*, 2022, **4**, 1158

PdPtRu nanocages with tunable compositions for boosting the methanol oxidation reaction†

Zihan Leng,[a] Xingqiao Wu,[a] Xiao Li,[a] Junjie Li,[a] Ningkang Qian,[a] Liang Ji,[a] Deren Yang [a] and Hui Zhang *[ab]

Received 29th November 2021
Accepted 5th January 2022

DOI: 10.1039/d1na00842k

rsc.li/nanoscale-advances

PtRu/C is a well-known commercial electrocatalyst with promising performance for the methanol oxidation reaction (MOR). Further improving the MOR properties of PtRu-based electrocatalysts is highly desirable, especially through structure design. Here we report a facile approach for the synthesis of PdPtRu nanocages with different components through a seed-mediated approach followed by chemical etching. The Pd@PtRu nanocubes were first generated using Pd nanocubes as the seeds and some Pd atoms were subsequently etched away, leading to the nanocages. When evaluated as electrocatalysts for the MOR in acidic media, the PdPtRu nanocages exhibited substantially enhanced catalytic activity and stability relative to commercial Pt/C and PtRu/C. Specifically, $PdPt_{2.5}Ru_{2.4}$ achieved the highest specific (8.2 mA cm^{-2}) and mass (0.75 mA mg_{Pt}^{-1}) activities for the MOR, which are 2.2 and 4.2 times higher than those of commercial Pt/C. Such an enhancement can be attributed to the highly open structure of the nanocages, and the possible synergistic effect between the three components.

Introduction

Faced with the aggravation of environmental pollution and continuous increase of energy demand, direct methanol fuel cells (DMFCs) are regarded as alternative energy conversion devices due to their high conversion efficiency, high energy density, and environment friendly characteristics.[1–5] In DMFCs, the methanol oxidation reaction (MOR) at the anode is conducted through multiple steps, resulting in slower reaction kinetics than electro-oxidation of hydrogen. Currently, Pt is proved to be the most effective single-metallic electrocatalyst with excellent activity and durability for the MOR.[6–8] However, scarce abundance and high cost of Pt severely limit its widespread use in DMFCs. Furthermore, Pt-based anodes are vulnerable to the poisoning effect associated with the CO-like intermediates during the MOR, leading to a dramatic loss of catalytic activity.[9–12] As such, designing highly active and strongly CO-tolerant Pt-based MOR electrocatalysts is critical to commercialize DMFCs widely.

Recently, tremendous efforts have been devoted to exploiting Pt-based nanocrystals through various strategies such as composition optimization, shape control, and structure design.[13–17] Combining Pt with other cheap metals to form binary or multimetallic alloys is considered as a promising method to improve the utilization efficiency of Pt, and thus reduce the loading of Pt as well. Simultaneously, the introduction of a second metal is demonstrated to tune the electron structure of Pt, thereby improving the activity and durability of Pt-based electrocatalysts.[18–21] Up to now, there are a rich variety of reports on the synthesis of PtM (M = Pd, Ru, Cu, Co, Ni, *etc.*) bimetallic alloys serving as electrocatalysts for the MOR.[22–25] Of them, PtRu alloys have received great attention as electrocatalysts for the MOR in acidic electrolytes, showing superior catalytic properties.[26–28] As an oxophilic metal, Ru can dissociate water to form the oxygenated species (*e.g.*, OH_{ads}) during the MOR. Such oxygenated species on Ru sites can oxidize and subsequently remove the CO_{ads} intermediates on Pt sites, resulting in the strong anti-poisoning capability of electrocatalysts.[29–31] For instance, Wang and coworkers reported the synthesis of the PtRu nanodendrites, showing substantially enhanced catalytic activity and stability towards the MOR as compared to PtRu nanocrystals and commercial Pt/C.[32] Despite the huge success in PtRu-based electrocatalysts, there is still a large room to improve the catalytic properties for the MOR, especially through the design of hollow nanostructures.

Hollow nanostructures have emerged as a new class of electrocatalysts due to the more abundant active sites and higher utilization efficiency of noble-metals compared to their solid counterparts. Among them, nanoframes and nanocages have received more attention due to the accessibility of reactants to both interior and exterior surfaces of electrocatalysts.[33–39] For example, Zhang *et al.* reported that PtCu nanoframes exhibited a MOR mass activity of 2.26 A mg_{Pt}^{-1} in

[a]*State Key Laboratory of Silicon Materials, School of Materials Science and Engineering, Zhejiang University, Hangzhou, Zhejiang 310027, P. R. China. E-mail: msezhanghui@zju.edu.cn*

[b]*Institute of Advanced Semiconductors, Hangzhou Innovation Center, Zhejiang University, Hangzhou, Zhejiang 310027, People's Republic of China*

† Electronic supplementary information (ESI) available. See DOI: 10.1039/d1na00842k

alkaline media, which was much higher than that of PtCu nanoparticles and commercial Pt/C.[40] In another study, AuPt bipyramid nanoframes were generated by a facile seed-mediated approach, showing substantially enhanced catalytic activity for the MOR relative to commercial Pt/C.[41] Recently, Xia *et al.* developed a promising approach for the synthesis of Pt-based nanocages with Pd nanocubes as the seeds.[42,43] However, synthesizing Pt-based hollow nanostructures with multimetallic components as MOR electrocatalysts is still challenging, in particular for those with well-defined exposed facets.

Here we report the synthesis of PdPtRu nanocages with different atomic ratios of Pt/Ru by a seed-mediated approach in combination with chemical etching. The PdPtRu nanocages exhibited substantially enhanced catalytic properties for the MOR compared to commercial Pt/C and PtRu/C. The $PdPt_{2.5}$-$Ru_{2.4}$ nanocages achieved the highest activity and durability because of the highly open structure and appropriately strong electron coupling arising from the three components.

Experimental section

Chemicals and materials

Poly(vinyl pyrrolidone) (PVP, $M_w \approx 55\,000$), ruthenium(III) chloride ($RuCl_3$, 99%), sodium hexachloroplatinate hexahydrate ($Na_2PtCl_6 \cdot 6H_2O$, 98%), ascorbic acid (AA, 99%), sodium tetrachloropalladate (Na_2PdCl_4, 98%), potassium bromide (KBr, 99%), aqueous hydrochloric acid (HCl) solution with a concentration of 37%, ferric chloride ($FeCl_3$, 97%), acetic acid (99.7%), and isopropyl alcohol (99.7%) were all purchased from Sigma-Aldrich. Acetone (99.5%), aqueous perchloric acid ($HClO_4$, PPT Grade, 70% in water), commercial Pt/C (20 wt%, *ca.* 3.2 nm Pt nanoparticles on Vulcan XC-72 carbon support), commercial PtRu/C (1 : 1, 20 wt%) and ethylene glycol (EG, 99%) were ordered from VWR, Veritas, Premetek Co., and J. T. Baker, respectively. To prepare the aqueous solutions, deionized water with a resistivity of 18.2 MΩ cm^{-1} at room temperature was used.

Synthesis of Pd nanocubes

Pd nanocubes with diameters of 13.8 nm were produced according to our previously reported method.[44] In a typical synthesis, an aqueous solution containing water (8 mL), KBr (300 mg), AA (60 mg), and PVP (105 mg) was added into a 20 mL vial, and then pre-heated at 80 °C in a magnetically stirred oil bath for 10 min. Subsequently, an aqueous solution consisting of water (3 mL) and Na_2PdCl_4 (57 mg) was added into the vial. After that, the vial was capped and heated at 80 °C for 3 h. Finallythe product was collected through centrifugation, washed three times with water, and then dispersed in EG at a concentration of 1.3 mg mL^{-1} for further use.

Synthesis of Pd@Pt–Ru core–shell nanocubes

In a standard synthesis, PVP (50 mg), AA (30 mg), KBr (50 mg), the suspension of Pd nanocubes (0.23 mL), and EG (3.7 mL) were mixed in a 20 mL vial and pre-heated at 110 °C. After 15 min, the temperature was raised rapidly to 200 °C within 15 min. After that, a solution containing EG (7 mL), $Na_2PtCl_6 \cdot 6H_2O$ (0.75 mg), and $RuCl_3$ (0.3 mg) was added into the vial at a rate of 1.0 mL h^{-1}. The vial was kept at 200 °C for 1 h. The final product was collected by centrifugation, washed once with acetone and twice with water, and then dispersed into water (1 mL) for further use.

Synthesis of PdPtRu nanocages

In a typical process, PVP (50 mg), KBr (300 mg), HCl (0.18 mL), $FeCl_3$ (30 mg), and water (6.5 mL) were mixed in a 20 mL vial, and heated at 95 °C. 1.0 mL of the Pd@Pt–Ru nanocube suspension was added into the vial using a pipette. After 2.5 h, the product was collected by centrifugation, and washed with water three times.

Morphological, structural, and compositional characterization

The morphology of the obtained sample was characterized by transmission electron microscopy (TEM) using a HITACHI HT-7700 microscope operated at 100 kV. X-ray photoelectron spectroscopy (XPS) was conducted on an ESCALAB 250Xi (Thermo, U.K.). The corresponding binding energies were calibrated with a C–C 1s peak of 284.5 eV. High-resolution TEM (HRTEM), high-angle annular dark-field scanning TEM (HAADF-STEM) and energy dispersive X-ray (EDX) mapping analyses were performed using a FEI Tecnai F20 G2 microscope operated at 200 kV. The atomic ratios of Pd, Pt and Ru in these samples were determined using inductively coupled plasma atomic emission spectrometry (ICP-AES, IRIS Intrepid II XSP, TJA Co., USA).

Electrochemical measurement

Electrochemical measurements were carried out in a three-electrode system at room temperature using a rotating disk electrode (RDE, Pine Research Instrumentation, USA) connected to an electrochemical workstation (CHI 760E). A reversible hydrogen electrode (RHE) was used as the reference electrode. The counter electrode was a Pt wire. To prepare the catalyst ink, 5 mg of PtRu/C or Pt/C catalysts were dispersed in 5 mL of a mixed solution and sonicated for 10 min. The solution contained a mixture of de-ionized water, isopropanol, and 5% Nafion on 117 solution at the volumetric ratio of 8 : 2 : 0.05. After that, 20 μL of the PtRu/C or Pt/C catalyst ink was added onto the RDE and dried under an air flow to make the working electrode. The geometric area of the RDE was 0.196 cm^2. The electrochemical active surface area (ECSA) was determined from the cyclic voltammogram (CV) curves, calculating the amount of charges by integrating the hydrogen desorption region after double layer correction. The CV measurement was performed in Ar-saturated 0.1 M $HClO_4$ solution at room temperature with a sweep rate of 50 mV s^{-1}. For the electrooxidation of methanol, CV curves were recorded in an Ar-purged 0.1 M $HClO_4$ and 0.5 M CH_3OH solution at a sweep rate of 50 mV s^{-1}. Chronoamperometric measurements of methanol oxidation were performed in

an Ar purged 0.1 M $HClO_4$ and 0.5 M CH_3OH solution at the front-peak positions of the forward curve for 1000 s.

Results and discussion

The PdPtRu nanocages were synthesized through a seed-mediated growth in combination with chemical etching (Scheme 1). First, the Pd@Pt_xRu ($x = 0.5$, 1, 2) nanocubes were generated by the co-deposition of Pt and Ru atoms using Pd nanocubes with an average diameter of ~13.8 nm as the seeds (Fig. S1†). Fig. S2† shows the TEM images of Pd@Pt_xRu nanocrystals, displaying a uniform cube-like shape (Fig. S2a, c and e†) and size distributions (~18 nm, Fig. S2b, d and f†). In the XRD patterns (Fig. S3†), all the diffraction peaks of the Pd@Pt_xRu nanocubes can be attributed to Pd or Pt with a face-centered cubic (fcc) structure. Taking Pd@PtRu as an example, the HRTEM, EDX mapping and line-scan analyses are shown in Fig. S4,† demonstrating the core–shell structure. Subsequently, the Pd core was selectively removed using HCl and $FeCl_3$ mixed solution. According to previous results,[42] the incorporation of Pd atoms into the PtRu overlayers could occur during the synthesis because of the interdiffusion between them as well as the co-reduction of Pd^{2+} ions resulting from the weak dissolution of Pd nanocubes at elevated temperature. Some Pd atoms embedded in the shell came in contact with the etchant and were etched away easily. As such, the removal of these embedded Pd atoms provides a pathway for the complete dissolution of the Pd core, leading to the formation of PdPtRu nanocages.

The morphology, structure, and composition of the Pt-based nanocages were characterized by the TEM, HRTEM, EDX mapping and line-scan analyses, as shown in Fig. 1. Clearly, most of the nanocrystals display a highly open structure with a cube-like shape and uniform size (Fig. 1a and S5†), indicating the formation of nanocages. The typical HRTEM image (Fig. 1b) of an individual nanocage shows well-resolved, ordered fringes in the same orientation, suggesting that the nanocage is a single crystal. The fringes with a lattice spacing of 0.19 nm can be indexed to the {100} planes of Pt-based alloys with a face-centered cubic (fcc) structure. In addition, the difference in contrast in the HRTEM image also confirms the hollow structure. The distribution of Pt, Ru and Pd in the nanocage is determined using EDX analysis (Fig. 1c and d). Clearly, the edges of the nanocages are composed of Pt, Ru, and Pd, while some Pd still exists in the inner side of the edges (Fig. 1c). This

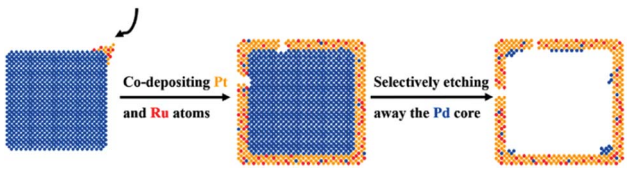

Scheme 1 Schematic illustration of the synthesis of the PdPtRu nanocages, including the co-deposition of Pt and Ru atoms on Pd nanocubes, and the selective removal of the Pd core *via* chemical etching.

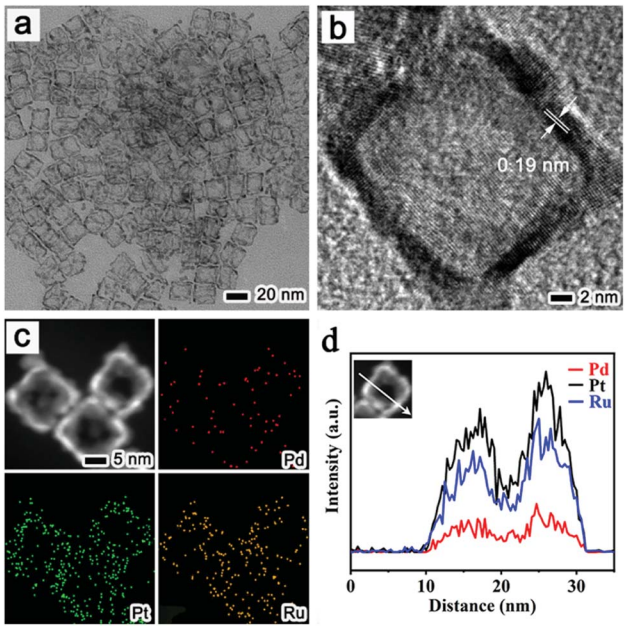

Fig. 1 Morphological, structural, and compositional characterization of the PdPtRu nanocages: (a) TEM image, (b) HRTEM image, (c) EDX mapping image, and (d) line-scan profiles.

demonstration is further supported by the EDX line-scan spectra (Fig. 1d). This result indicates that Pd atoms were not totally etched but partly kept instead. As such, the interior of the nanocage is Pd rich, while Pt and Ru were distributed uniformly at the surface. The atomic ratio of Pt/Ru was about 1 : 2.5 : 2.4 as quantitatively determined by ICP-AES analysis (Table S1†), which is close to the EDX result (Table S2†). For simplicity, this sample was defined as standard one and labelled as $PdPt_{2.5}Ru_{2.4}$.

This method can be extended to synthesize other PdPtRu nanocages with different compositions by tuning the amount of Pt and Ru precursors. When the feed ratio of Pt/Ru was varied to 2 or 0.5, hollow nanostructures with a cubic shape and similar size were still achieved (Fig. S6 and S7†). The big difference of these two samples from the standard one is the atomic ratio of Pt/Ru according to EDX analysis (Table S2†). The quantitative composition of these two samples was measured by ICP-AES analysis (Table S1†). Accordingly, these two samples were labelled as $PdPt_{7.3}Ru_{3.6}$ and $PdPt_{3.7}Ru_{8.1}$.

The valence and electronic states of the three PdPtRu nanocages were analyzed using the XPS technique, as shown in Fig. S8.† As observed, Pt, Ru and Pd exist mainly in the zerovalent state for such three samples, indicating that the metallic state is the majority. In addition, there is an obvious positive shift of Pt 4f and Pd 3d and an obvious negative shift of Ru 3p in these three nanocages compared to those of the corresponding bulk materials. Taking $PdPt_{2.5}Ru_{2.4}$ nanocages as an example (Fig. S8a†), the binding energies of Pt^0 are located at 71.6 ($4f_{7/2}$) and 74.9 ($4f_{5/2}$) eV, respectively, displaying a positive shift compared with bulk Pt 4f peaks at 71.20 ($4f_{7/2}$) and 74.53 eV ($4f_{5/2}$). Simultaneously, the binding energies of Ru^0 are located at 462.8 ($3p_{1/2}$) and 485.1 ($3p_{5/2}$) eV, respectively,

showing a negative shift compared with bulk Ru 3p peaks at 463.3 ($3p_{1/2}$) and 485.6 eV ($3p_{3/2}$). This result demonstrates the occurrence of electron transfer between Pt, Pd and Ru. Due to the possible interaction between the three elements in the PdPtRu nanocages, this effect might weaken the adsorption of partial oxidation intermediates (*e.g.*, CO) on Pt, thereby improving the catalytic activity for the MOR by alleviating the CO poisoning.[45,46]

These three PdPtRu nanocages were then loaded on a carbon support (Vulcan XC-72R, Fig. S9†), and then evaluated as the catalysts for the MOR with commercial Pt/C and PtRu/C as references. Fig. S10† shows the cyclic voltammetry (CV) curves of these five catalysts including commercial Pt/C and PtRu/C recorded in Ar-purged 0.1 M $HClO_4$ solution at a sweep rate of 100 mV s^{-1}. As determined by the hydrogen desorption region (0.05–0.4 V) in the CV curves, the electrochemically active surface areas (ECSAs) of the $PdPt_{2.5}Ru_{2.4}$, $PdPt_{3.7}Ru_{8.1}$ and $PdPt_{7.3}Ru_{3.6}$ nanocages are 59.4, 67.5 and 64.4 $m^2\ g_{Pt}^{-1}$, respectively, larger than that of Pt/C (55.3 $m^2\ g_{Pt}^{-1}$) and PtRu/C (42.8 $m^2\ g_{Pt}^{-1}$) due to the highly open structure (Table S3†). This demonstration is also supported by CO-stripping measurement (Fig. 3 and Table S3†). Fig. 2a and b compare the CV curves of these catalysts for the MOR performed in the solution containing 0.1 M $HClO_4$ and 0.5 M CH_3OH at a sweep rate of 50 mV s^{-1}. Obviously, the nanocages exhibited higher specific and mass activities relative to commercial Pt/C and commercial PtRu/C due to their unique structure and synergetic effect of multiple components. In addition, the MOR activities of the nanocages followed the sequence: $PdPt_{3.7}Ru_{8.1}$ < $PdPt_{7.3}Ru_{3.6}$ < $PdPt_{2.5}Ru_{2.4}$ (Fig. S11†). Specifically, the $PdPt_{2.5}Ru_{2.4}$ nanocages showed the highest mass (0.75 mA mg_{Pt}^{-1}) and specific (8.2 mA cm^{-2}) activities towards the MOR, which are 4.2 and 2.2 times higher than those of commercial Pt/C (0.18 mA mg_{Pt}^{-1} and 3.8 mA cm^{-2}), respectively (Fig. 2c). In addition, the $PdPt_{2.5}Ru_{2.4}$ nanocages outperformed most of the previously reported Pt-based MOR electrocatalysts in acid media (Table S4†).

The superior catalytic activities of the nanocages can be understood based on two reasons. (i) The bifunctional mechanism and ligand effect. As is well known, Pt is the active site for methanol adsorption and dissociation during the MOR, causing the formation of intermediates mainly including CO_{ads}. Such CO_{ads} intermediates can severely poison active sites of Pt through strong adsorption, and finally deactivate Pt-based electrocatalysts. The incorporation of Ru and Pd can cause a down shift of the d-band center of Pt (ligand effect),[47] thereby reducing the binding strength of Pt with the adsorbed intermediates (*e.g.*, CO) and enhancing the tolerance to CO poisoning. The addition of Ru and Pd with the oxophilic capability also promotes the removal of CO_{ads} intermediates during the catalytic reaction, and thus substantially enhances the activity by inhibiting the CO poisoning (bifunctional mechanism).[48] (ii) The structural effect. ECSA data (Table S3†) and HRTEM image (Fig. 1b) indicate that the nanocages usually contain lots of low-coordinated sites on the surface. These low-coordinated sites are active for the MOR, which might be responsible for the better MOR activity.[49]

To further confirm the alleviation of CO poisoning in the PdPtRu nanocages, the CO stripping of the three catalysts including $PdPt_{2.5}Ru_{2.4}$/C, PtRu/C, and Pt/C was tested in 0.1 M $HClO_4$ with CO flow, as shown in Fig. 3. As observed, the peak potentials for CO oxidation on $PdPt_{2.5}Ru_{2.4}$/C, PtRu/C, and Pt/C are 0.60, 0.61, and 0.88 V, respectively, showing a negative shift of 28 mV for $PdPt_{2.5}Ru_{2.4}$/C relative to Pt/C. This result indicates that the addition of Ru and Pd effectively promotes the oxidation of CO and dramatically alleviate the CO poisoning.

The electrocatalytic stability of the PdPtRu/C including commercial PtRu/C and Pt/C catalysts for the MOR was investigated by the long-term current–time (*I*–*t*) measurement technique, as shown in Fig. 2d and S11d.† As can be seen, the PdPtRu/C catalysts show higher steady current density relative

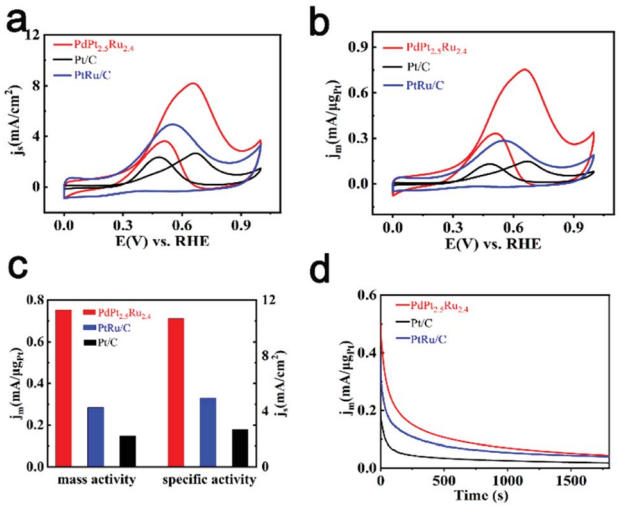

Fig. 2 (a and b) Cyclic voltammograms (CVs) of three different catalysts including $PdPt_{2.5}Ru_{2.4}$ nanocages (red), commercial Pt/C (black) and commercial PtRu/C (blue) for the MOR normalized by the ECSA and Pt mass, respectively. (c) Specific and mass activity at the peak position of the forward curve. (d) Current–time curves (*I*–*t*) for methanol electrooxidation of these three catalysts at the peak position voltage (*vs.* RHE) for 1800 s.

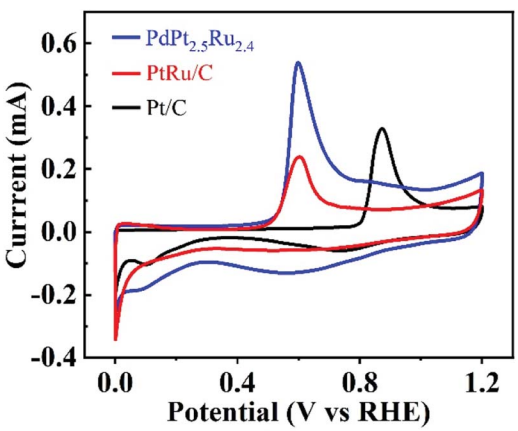

Fig. 3 CO stripping voltammograms of three different catalysts including $PdPt_{2.5}Ru_{2.4}$ nanocages (red), commercial Pt/C (black) and commercial PtRu/C (blue) recorded in 0.1 M $HClO_4$ aqueous solution.

to commercial PtRu/C and Pt/C for the MOR over the entire time range, especially the $PdPt_{2.5}Ru_{2.4}$/C catalyst. In order to further confirm the excellent MOR activity and durability of PdPtRu/C, the electrocatalytic test was conducted in 0.1 M $HClO_4$ and 1 M CH_3OH, as shown in Fig. S12.† Compared to Pt/C and PtRu/C, the catalytic activity of $PdPt_{2.5}Ru_{2.4}$/C was improved significantly. This data also showed that the $PdPt_{2.5}Ru_{2.4}$ nanocages had better tolerance for CO poisoning independent of the methanol concentration. Such superior durability can be attributed to weaker CO adsorption on the nanocages and better CO tolerance due to the addition of oxophilic Ru and Pd. After the stability test, the three PdPtRu/C catalysts were characterized by the TEM technique, as shown in Fig. S13.† As observed, the nanocages were kept unchanged and still well-dispersed on the carbon support, indicating that their high structural stability is also responsible for the enhanced catalytic durability. However, the Pt/C and PtRu/C catalysts exhibited some degree of aggregation, which was also responsible for the degradation of MOR activity during the stability test.

Conclusions

In summary, we have developed a facile approach to synthesize PdPtRu nanocages with tunable compositions. Such nanocages were generated through two steps including the formation of Pd@PtRu nanocrystals and partial etching of Pd. The PdPtRu nanocages exhibited substantially enhanced catalytic activity and stability for the MOR relative to commercial PtRu/C and Pt/C, with the $PdPt_{2.5}Ru_{2.4}$ nanocages being the best catalyst. This enhancement can be attributed to the bifunctional mechanism and ligand effect arising from incorporation of Ru and Pd as well as the unique hollow structure. This work not only provides a facile method for the synthesis of PtRu-based MOR catalysts with a highly open structure, but also offers a great opportunity to design catalysts with enhanced performance for a rich variety of potential applications.

Conflicts of interest

The authors declare that they have no conflict of interest.

Acknowledgements

The work on electron microscopy was carried out in the Center for Electron Microscopy of Zhejiang University. This work was supported by the National Science Foundation of China (51522103, 51871200, and 61721005) and National Program for Support of Top-notch Young Professionals.

Notes and references

1 N. V. Long, Y. Yang, M. T. Cao, N. V. Minh, Y. Cao and M. Nogami, *Nano Energy*, 2013, **2**, 636–676.
2 T. Cochell, W. Li and A. Manthiram, *J. Phys. Chem. C*, 2013, **117**, 3865–3873.
3 X. Zhao, J. Zhang, L. J. Wang, H. Li, Z. Liu and W. Chen, *ACS Appl. Mater. Interfaces*, 2015, **7**, 26333–26339.
4 F. Lyu, M. Cao, A. Mahsud and Q. Zhang, *J. Mater. Chem. A*, 2020, **8**, 15445.
5 N. Gao, X. Wu, X. Li, J. Huang, D. Li, D. Yang and H. Zhang, *RSC Adv.*, 2020, **10**, 12689.
6 S. F. Xue, W. T. Deng, F. Yang, J. Yang, I. S. Amiinu, D. He, H. Tang and S. Mu, *ACS Catal.*, 2018, **8**, 7578–7584.
7 J. Lan, K. Wang, Q. Yuan and X. Wang, *Mater. Chem. Front.*, 2017, **1**, 1217–1222.
8 Y. Xiong, Y. Ma, J. Li, J. Huang, Y. Yan, H. Zhang, J. Wu and D. Yang, *Nanoscale*, 2017, **9**, 11077–11084.
9 N. K. Chaudhari, Y. Hong, B. Kim, S. Choi and K. Lee, *J. Mater. Chem. A*, 2019, **7**, 17183–17203.
10 G. Xu, R. Sui, J. Liu, L. Zhang, X. Gong, R. Gao, B. Liu and J. Zhang, *J. Mater. Chem. A*, 2018, **6**, 12759–12767.
11 B. Lu, T. Sheng, N. Tian, Z. Zhang, C. Xiao, Z. Cao, H. Ma, Z. Zhou and S. Sun, *Nano Energy*, 2017, **33**, 65–71.
12 L. Lu, S. Chen, S. Thota, X. Wang, Y. Wang, S. Zou, J. Fan and J. Zhao, *J. Phys. Chem. C*, 2017, **121**, 19796–19806.
13 C. Li, X. Chen, L. Zhang, S. Yan, A. Sharma, B. Zhao, A. Kumbhar, G. Zhou and J. Fang, *Angew. Chem., Int. Ed.*, 2021, **60**, 7675–7680.
14 T. Bian, B. Sun, S. Luo, L. Huang, S. Su, C. Meng, S. Su, A. Yuan and H. Zhang, *RSC Adv.*, 2019, **9**, 35887.
15 X. Li, Y. Zhou, Y. Du, J. Xu, W. Wang, Z. Chen and J. Cao, *Int. J. Hydrogen Energy*, 2019, **44**, 18050–18057.
16 T. Kwon, M. Jun, H. Y. Kim, A. Oh, J. Park, H. Baik, S. H. Joo and K. Lee, *Adv. Funct. Mater.*, 2018, **28**, 1706440.
17 J. Zhu, M. Xie, Z. Chen, Z. Lyu, M. Chi, W. Jin and Y. Xia, *Adv. Energy Mater.*, 2020, **10**, 1904114.
18 Y. Pan, H. Li, Z. Wang, Y. Han, Z. Wu, X. Zhang, J. Lai, L. Wang and S. Feng, *Chem. Commun.*, 2020, **56**, 9028.
19 F. Wu, J. Lai, L. Zhang, W. Niu, B. Lou, R. Luque and G. Xu, *Nanoscale*, 2018, **10**, 9369–9375.
20 B. Sun, L. Huang, S. Su, S. Luo, C. Meng, H. M. A. Basit, J. Xiao, T. Bian and S. Su, *Mater. Chem. Phys.*, 2020, **252**, 123234.
21 A. Shan, S. Huang, H. Zhao, W. Jiang, X. Teng, Y. Huang, C. Chen, R. Wang and W. Lau, *Nano Res.*, 2020, **13**, 3088–3097.
22 H. An, Z. Zhao, Q. Wang, L. Zhang, M. Gu and C. Li, *ChemElectroChem*, 2018, **5**, 1345–1349.
23 F. Luo, Q. Zhang, K. Qu, L. Guo, H. Hu, Z. Yang, W. Cai and H. Cheng, *ChemCatChem*, 2019, **11**, 1238–1243.
24 S. Lu, K. Eid, D. Ge, J. Guo, L. Wang, H. Wang and H. Gu, *Nanoscale*, 2017, **9**, 1033.
25 C. Shang, Y. Guo and E. Wang, *J. Mater. Chem. A*, 2019, **7**, 2547.
26 S. Lu, H. Li, J. Sun and Z. Zhuang, *Nano Res.*, 2018, **11**, 2058–2068.
27 L. Zhang, A. Gao, Y. Liu, Y. Wang and J. Ma, *Electrochim. Acta*, 2014, **132**, 416–422.
28 J. Guo, G. Suna, S. Suna, S. Yan, W. Yang, J. Qi, Y. Yan and Q. Xin, *J. Power Sources*, 2017, **168**, 299–306.
29 D. Chen and Y. J. Tong, *Angew. Chem., Int. Ed.*, 2015, **54**, 9394–9398.
30 J. Zhang, X. Qu, Y. Han, L. Shen, S. Yin, G. Li, Y. Jiang and S. Sun, *Appl. Catal., B*, 2020, **263**, 118345.

31 C. Kuo, I. Lua, L. Chang, Y. Hsieh, Y. Tsengand, P. Wu and J. Lee, *J. Power Sources*, 2013, **240**, 122–130.
32 S. Lu, K. Eid, D. Ge, J. Guo, L. Wang, H. Wang and H. Gu, *Nanoscale*, 2017, **9**, 1033.
33 H. Yin, Z. Zhang, Y. Guo, K. Yuan and Y. Zhang, *Mater. Chem. Front.*, 2020, **4**, 1985.
34 S. Chen, M. Li, M. Gao, J. Jin, M. A. Spronsen, M. B. Salmeron and P. Yang, *Nano Lett.*, 2020, **20**, 1974–1979.
35 T. Yang, J. Ahn, S. Shi, P. Wang, R. Gao and D. Qin, *Chem. Rev.*, 2021, **121**, 796–833.
36 Z. Wang, L. Huang, Z. Tian and P. Shen, *J. Mater. Chem. A*, 2019, **7**, 18619.
37 N. Becknell, Y. Son, D. Kim, D. Li, Y. Yu, Z. Niu, T. Lei, B. T. Sneed, K. L. More, N. M. Markovic, V. R. Stamenkovic and P. Yang, *J. Am. Chem. Soc.*, 2017, **139**, 11678–11681.
38 F. Nosheen, Z. Zhang, J. Zhuang and X. Wang, *Nanoscale*, 2013, **5**, 3660–3663.
39 S. Chen, Z. Niu, C. Xie, M. Gao, M. Lai, M. Li and P. Yang, *ACS Nano*, 2018, **12**, 8697–8705.
40 Z. Zhang, Z. Luo, B. Chen, C. Wei, J. Zhao, J. Chen, X. Zhang, Z. Lai, Z. Fan, C. Tan, M. Zhao, Q. Lu, B. Li, Y. Zong, C. Yan, G. Wang, Z. J. Xu and H. Zhang, *Adv. Mater.*, 2016, **28**, 8712–8717.
41 C. Fang, G. Zhao, Z. Zhang, Q. Ding, N. Yu, Z. Cui and T. Bi, *Chem.–Eur. J.*, 2019, **25**, 7351–7358.
42 L. Zhang, L. Roling, X. Wang, M. Vara, M. Chi, J. Liu, S. Choi, J. Park, J. Herron, Z. Xie, M. Mavrikakis and Y. Xia, *Science*, 2015, **349**, 412–416.
43 X. Wang, L. Figueroa-Cosme, X. Yang, M. Luo, J. Liu, Z. Xie and Y. Xia, *Nano Lett.*, 2016, **16**, 1467–1471.
44 M. Jin, H. Liu, H. Zhang, Z. Xie, J. Liu and Y. Xia, *Nano Res.*, 2011, **4**, 83–91.
45 T. Kwon, M. Jun and K. Lee, *Adv. Mater.*, 2020, **32**, 2001345.
46 H. Cheng, Z. Cao, Z. Chen, M. Zhao, M. Xie, Z. Lyu, Z. Zhu, M. Chiand and Y. Xia, *Nano Lett.*, 2019, **19**(8), 4997–5002.
47 W. Li, Y. Zhao, Y. Liu, M. Sun, G. I. N. Waterhouse, B. Huang, K. Zhang, T. Zhang and S. Lu, *Angew. Chem., Int. Ed.*, 2021, **60**, 3290–3298.
48 T. Yajima, H. Uchida and M. Watanabe, *J. Phys. Chem. B*, 2004, **108**, 2654–2659.
49 Y. Xiong, H. Shan, Z. Zhou, Y. Yan, W. Chen, Y. Yang, Y. Liu, H. Tian, J. Wu, H. Zhang and D. Yang, *Small*, 2017, **13**, 1603423.